Modeling the Impact of Pre-Flushing on CTE in Proton Irradiated CCD-based Detectors

R. H. Philbrick[1]

Abstract

A software model is described that performs a "real world" simulation of the operation of several types of CCD-based detectors in order to accurately predict the impact that high-energy proton radiation has on image distortion and MTF. The model was written primarily to predict the effectiveness of vertical pre-flushing on the custom full frame CCD-based detectors intended for use on the proposed *Kepler* Discovery mission, but it is capable of simulating many other types of CCD detectors and operating modes as well. The model keeps track of the occupancy of all P-V, V-V, and O-V defect centers under every CCD electrode over the entire detector area. The integrated image is read out by simulating every electrode-to-electrode charge transfer in both the vertical and horizontal CCD registers. A signal level dependency on the capture and emission of signal is included and the current state of each electrode (e.g. barrier or storage) is considered when distributing integrated and emitted signal. Options for performing pre-flushing, pre-flashing, and including mini-channels are available on both the vertical and horizontal CCD registers. In addition, dark signal generation and image transfer smear can be selectively enabled or disabled. A comparison of the CTE data measured on the Hubble STIS CCD with the CTE extracted from model simulations of the STIS CCD show good agreement.

I. INTRODUCTION

It has been well established in the radiation effects community that CCD (Charge-Coupled Device)-based detectors suffer degraded Charge Transfer Efficiency (CTE) performance after being exposed to high-energy proton radiation [1-4]. The properties of the silicon lattice defect centers (a.k.a. electron traps, or traps for short) created by high energy proton radiation have been extensively studied and the results indicate that such traps have strong dependencies on signal level, clocking speeds, dwell time, and operating temperature [4]. As a result of these dependencies, each pixel in an arbitrary two-dimensional image can have a different CTE and, further, the CTE can vary with changes in the incident image (i.e. from scene to scene). This fact makes predicting the image distortion and the Modulation Transfer Function (MTF) resulting from degraded CTE performance in an arbitrary image a difficult task.

Significant ground based characterization of CTE in irradiated CCDs has been performed using low energy radioactive sources such as Fe^{55}. While this type of characterization has produced a great deal of revealing information on the properties of the proton induced traps, the CTE values calculated from such experiments do not provide sufficient information for predicting the impact that radiation-induced transfer inefficiencies have on arbitrary images. CTE models such as those presented by Dale et al. [2], Gallagher et al. [5], and Janesick [6] can, with good accuracy, match the measured CTE response (using an Fe^{55} source) from pre and post proton irradiated CCDs, thereby validating the assumed trap properties. However, it will be

[1] Ball Aerospace & Technologies Corp., PO Box 1062, MS CO-5, Boulder CO, 80306.

shown that using the CTE values from such models to predict the image degradation (e.g. distortion or MTF) in an arbitrary image can yield inaccurate results.

II. SOFTWARE MODEL

The software model presented herein performs a "real world" simulation of the operation of several types of CCD-based detectors with the goal of yielding accurate predictions of image distortion and MTF resulting from exposure to high-energy proton radiation. (The model, called "*Trapper*," was written primarily to predict the effectiveness of vertical pre-flushing on the custom CCD detectors intended for use on the proposed *Kepler* Discovery mission [7]. However, it is capable of simulating many other types of CCD-based detectors and operating modes as well.) The model keeps track of the occupancy of all P-V (Phosphorous – Silicon), V-V (Divacancy), and O-V (Oxygen – Silicon) traps under every CCD electrode over the entire two-dimensional detector during both the integration and readout periods over any number of frames. The integrated image is read out by simulating every electrode-to-electrode transfer in both the vertical and horizontal CCD registers.

Prior to the start of the simulation, all traps are either totally emptied to simulate a new exposure condition or totally filled to simulate an immediate power on condition. For applications where dynamic scenes are to be continuously imaged or where single exposures are to be taken, the first option is preferred. The trap population level in these applications never reaches a steady state condition and the first frame out of the simulation model should be used for performing CTE and MTF calculations. The term steady state is used here to describe the output image content. Specifically, steady state is achieved when, under the condition of a static input image, the output image no longer changes over time. Significant differences can be observed in the image content between the first and subsequent images out of the model and, hence, it is vital that the proper model be chosen to most closely match the detector application. In applications where a static scene is to be imaged over multiple frames (e.g. *Kepler*), the initial condition is not important so long as a sufficient number of frames are simulated, thereby ensuring the trap population level has reached a steady state condition. For the *Kepler* detector a steady state condition was achieved after 2 to 3 frames were read out of the detector.

A designated image integration period, wherein the incident image is integrated along with dark signal, precedes the readout of each frame. For the *Kepler* application a specific simulated star pattern was used, although any other image can be used, as well as simulated horizontal or vertically oriented sinusoidal images for the determination of MTF (not discussed here). Prior to the start of each electrode-to-electrode transfer the appropriate dark signal, background signal, and image signal is added to each electrode and then distributed between the two adjacent storage electrodes. In shuttered systems the integrated image will be zero during the frame readout period; thereby yielding zero image transfer smear. For frame transfer or full frame CCD-based detectors operating with no external shutter (e.g. *Kepler* detector), the model accurately accounts for image transfer smear.

Once the image scene is integrated a vertical electrode-to-electrode charge transfer is performed followed by a trap capture and emission simulation. At the conclusion of a complete vertical transfer cycle (e.g. 4 electrode-to-electrode transfers for a 4 phase CCD), the readout of the serial CCD is simulated. As with a real CCD, the net pixel signal presented at the output of the charge-to-voltage conversion amplifier is comprised of the signal from all corresponding serial CCD electrodes, which includes the signal from the storage electrode and the emitted signal from the storage and barrier electrodes. The above vertical transfer cycle is repeated until the entire image is read out, then the entire frame cycle is repeated for the requested number of read out frames.

The model also supports the options for electrically injecting signal into either the vertical or horizontal CCDs (i.e., rows and/or columns) and for adding a background signal (a.k.a. "fat zero"). Electrical injection can be used to pre-flush the CCD with an artificial signal with the goal of keeping the radiation-induced traps fully populated while the integrated (real) signal is read out. The background signal option can be used to simulate the pre-flashing of the vertical CCD register, a process wherein a pseudo uniform low level signal is added to the entire vertical CCD to fill traps exposed by low signal levels, or to simulate the intensity of the background image.

The simulation of trap emission and capture is accomplished by first calculating the number of exposed traps under each barrier and storage electrode for each trap type (e.g. P-V or V-V). An exposed trap is one that is capable of capturing signal. Using information gathered from previous work [8], a square root relationship between the number of exposed traps under an electrode and the signal level has been adopted. Specifically, the number of exposed traps (n_{ex}) under a given electrode is assumed to vary as

$$n_{ex} = (1 - r_o) \cdot n_t \cdot \sqrt{\frac{N_{sig}}{N_{sat}}} + r_o \cdot n_t \qquad (1)$$

where N_{sig} is the signal, r_o is the fraction of traps exposed with zero signal present, n_t is the total trap population under the electrode, and N_{sat} is the saturation signal level under the electrode. When mini-channels are employed and the signal level is less than the mini-channel capacity, n_t in Equation 1 is replaced with the mini-channel trap population (n_{mc}), and N_{sat} is replaced with the mini-channel signal capacity ($N_{sat\text{-}mc}$). When the signal level is greater than the mini-channel capacity, Equation 1 becomes

$$n_{ex} = (1 - r_o) \cdot n_{mt} \cdot \sqrt{\frac{N_{sig}}{N_{sat}}} + r_o \cdot n_{mt} + n_{mc} \qquad (2)$$

where $n_{mt} = n_t - n_{mc}$, and n_{mc} is the trap population of the mini-channel, which is approximated as $n_t \cdot L_{mc} \div L_{hp}$ (where L_{mc} is the width of the mini-channel and L_{hp} is the horizontal pixel pitch). When mini-channels are employed and the signal is equal to the mini-channel capacity, Equation 1 simplifies to $n_{ex} = n_{mc}$ as expected. Equations 1 and 2 are plotted in Figure 1 to show the impact on trap exposure of varying signal level. The discontinuity in the mini-channel curve occurs at the capacity of the mini-channel. This type of function was chosen to account for the differences in signal volume between the two cases (i.e., mini-channel versus no mini-channel). For signal levels slightly greater than the mini-channel capacity, the relative number of exposed traps is therefore assumed to be greater than the non mini-channel case to account for the extra volume of the mini-channel.

The number of empty traps (i.e., unpopulated traps) under each electrode is then determined by subtracting the number of occupied traps (n_{filled}) from the current total of exposed traps under the particular electrode and for the particular trap type. The condition when n_{empty} is greater than zero means there are unpopulated (exposed) traps under the electrode and the number that become populated (capture electrons) is

$$n_{pop} = \begin{Bmatrix} n_{empty} \cdot P_{cn} \text{ ; for } N_{sig} \geq n_{empty} \\ N_{sig} \cdot P_{cn} \text{ ; for } N_{sig} < n_{empty} \end{Bmatrix} . \qquad (3)$$

Conversely, the condition when n_{empty} is less than zero means there are populated (exposed) traps under the electrode and the number that become unpopulated (give up electrons) is

$$n_{unpop} = \begin{Bmatrix} -n_{empty} \cdot P_{en} \text{ ; if storage phase} \\ +n_{filled} \cdot P_{en} \text{ ; if barrier phase} \end{Bmatrix} \qquad (4)$$

where the probability that an unpopulated exposed trap will be filled (P_{cn}) and the probability that a populated trap will emit (P_{en}) within a period T_d are given by [2]

$$P_{cn} = 1 - e^{-\frac{T_d}{\tau_{cn}}} \text{ , and } \quad P_{en} = 1 - e^{-\frac{T_d}{\tau_{en}}} \qquad (5)$$

respectively, where τ_{cn} is the capture time constant and τ_{en} is the emission time constant associated with trap type *n*. The signal level and number of populated traps are then adjusted to reflect the capture and emission results from Equations 3 and 4. Since no 'free' signal is retained under barrier electrodes, any signal generated in or emitted from these areas is assumed to divide evenly between the two adjacent storage electrodes. While this approach can result in fractional charges, it is assumed that the cumulative effect over the relatively large number of transfers is negligible. In the case of 4 phase CCDs, where 2 phases are used to form the storage region, the signal is evenly divided between the 4 adjacent storage phases (i.e. 2 to the left and 2 to the right), as illustrated in Figure 2. The general flow of the *Trapper* modeling program is depicted in Figure 3.

The capture time constant for each trap type was calculated using

$$\tau_{cn} = \left(\sigma_n \nu_{th} n_s\right)^{-1} \tag{6}$$

where σ_n is the capture cross section, ν_{th} is the average thermal velocity of the mobile electrons, and n_s is the signal density. Given that considerable uncertainty exists in the determination of n_s, measured data was sought out for τ_{cn}, with limited success. Some data for τ_{cn} for the P-V trap was found in M. Robbins et al. [13], but no data was uncovered for the O-O and V-V traps. Using Equation 6 and a signal level of 1620 e^-, τ_{cn} was calculated for each of the trap types (at –90°C) to be 911 ns for the O-V and V-V traps and 650 ns for the P-V trap. The values reported by Robbins et al. [13] were based on measurements taken at -23°C and they ranged from 100 to 500 ns. At -23°C, Equation 6 predicts a capture constant of approximately 555 ns, which is in general agreement with the values from Robbins. Using a signal dwell period of 121 μs and a capture constant of 911 ns, Equation 5 yields a value of unity and, therefore, the capture time constant is not expected to significantly impact the CTE performance of the detector in the *Kepler* application.

The emission time constants for each trap type was calculated using

$$\tau_{en} = \left(\sigma_n \mathrm{X}_n \nu_{th} N_c \exp(\frac{-E_{gn}}{kT}) \right)^{-1} \tag{7}$$

where X_n is the entropy factor [3], N_c is the effective density of states in the conduction band, and E_{gn} is the band gap associated with trap of type n. The quantity $\nu_{th}N_c$ is calculated using [11]

$$\nu_{th}N_c = 4.11\mathrm{x}10^{25} \cdot \left(\frac{T}{77}\right)^2 \tag{8}$$

and the values for $\sigma_n X_n$ listed in Table 1 were arrived at using both measured data and through comparisons with measured emission time constant data [5,6,10].

III. SETUP AND VALIDATION OF MODEL

To determine r_o (in Equation 1), several modeling runs were performed to simulate a ground-based radiation experiment performed by Ball Aerospace & Technologies Corp. in 1997. In this experiment SITe-502 backside illuminated CCD detectors were exposed to a proton fluence of 5.4E10 p/cm^2 (using 63 MeV protons) sufficient to yield a Non-Ionizing Energy Loss (NIEL) [12] of 1.8E8 MeV/g. The SITe-502 device is a 512 x 512 full frame detector with dual readout. During the experiment the CTE was measured using a radioactive Fe^{55} source as the input image and the results (at –90°C) indicated a parallel CTE of 0.9990 per pixel. The modeling program was setup with the SITe-502 device parameters and the identical clocking scheme used in the ground experiment. To simulate the image produced by the Fe^{55} source, a single column image was created with simulated particle hits spaced every 50 rows. The hits were varied in signal intensity, except for the principal target pixel in row 500, which was given an exact signal intensity of 1620 electrons (e^-). It was assumed that the trap population level in the SITe-502 detector reached steady state based on the fact that the CTE measurement was performed repeatedly over a period of time. The results from the simulations showed a value of r_o

= 0.28 yielded an exact match to the measured CTE data and, therefore, this value was adopted.

To test the accuracy of the model, the CCD-based detector used on the Hubble STIS instrument was modeled using data obtained from the Space Telescope Science Institute [9]. The STIS detector is a 1k x 1k quad readout, full frame detector with 21 μm x 21 μm pixels that employ a 3-phase CCD architecture. Although it is not identical to the SITe-502 device used in the ground-based experiment previously mentioned, both the STIS and SITe-502 detectors were fabricated using the same standard manufacturing process. The signal levels (~2ke$^-$) for both the ground-based and STIS cases were small compared to the saturation levels, but it is believed the model presented herein will be equally valid for higher signal levels.

After 2.6 years on orbit the measured CTI (1 - CTE) ranged between 0.78E-4 and 1.94E-4 per pixel for signal levels between 200 and 400 e$^-$ and background levels of 3 to 14 e$^-$ (per pixel). The signal levels represent summed values over a 7 x 7 pixel aperture with the detector operated at –83°C. The ground estimate of the total NIEL on the STIS CCD detector after 2.6 years is ~1.29E7 MeV/g. The trap densities corresponding to this level of NIEL were estimated to be 2.58E9 #/cm^3 for P-V and 5.16E9 #/cm^3 for the V-V using expressions developed by M. Robbins [10]. In addition, an O-V trap density of 3.87E9 #/cm^3 was used based on a linear scaling (with NIEL) of data reported by D. Gallagher [5].

The input image consisted of two Gaussian shaped stars located at rows 500 and 990, each having a radius of 3 pixels, with the maximum signal in the center pixel being 100 e$^-$ for row 990 and 50 e$^-$ for row 500. The total signal input for the star centered over row 990 was 314 e$^-$ and the background signal was set to be 5 e$^-$ per pixel. To reduce the simulation time, only a 20 column by 1024 row section of the STIS detector was modeled. This simplification does not impact the accuracy of the parallel CTE estimates and significantly reduced the simulation run time. The simulation of the STIS CCD detector yielded a CTI value of 1.94E-4, which is consistent with the measured values.

IV. MODELING OF THE KEPLER DETECTOR

The *Kepler* CCD-based detector is a thinned, backside illuminated 2200 column by 1024 row full frame device with 27 μm x 27 μm pixels, as depicted in Figure 4. A 4-phase CCD architecture is used in both the horizontal and vertical CCD registers to maximize signal capacity and minimize clock induced noise. Readout amplifiers exist at both ends of the serial CCD shift register, which also supports bi-directional charge transfer. A vertical injection circuit is located adjacent to the last row (i.e., the row furthest from the serial CCD). Each *Kepler* CCD will be used to monitor the relative signal intensity of ~4k stars ranging in magnitude (m_v) from 14 to 9. The optical system is designed to purposely defocus each star image onto an approximate 5 x 5 pixel aperture. Assuming the stars are randomly distributed across the active area, the CCD will have ~2 stars centered over each column. Numerous lower intensity stars will result in a minimum background signal of ~200 electrons (e$^-$) in every pixel over the nominal 2.5 second integration period. A vertical injection circuit located adjacent to the last row enables a metered amount of signal to be injected into each column. The injection circuit can be used to pre-flush the active area of the CCD with the goal of filling a high percentage of the radiation induced traps and allowing subsequent image signal to be read out with minimal distortion. Additional details on the operation of the *Kepler* CCDs are summarized in Table 1.

From Equation 5, it is concluded that the longer signal is resident under an electrode the greater the probability that a portion of that signal will become captured by radiation induced traps. Given this relationship, and the knowledge that the vertical (row-to-row) and horizontal (pixel-to-pixel) clocking periods for the *Kepler* CCDs are 484 μs and 333 ns, respectively, the CTE in the vertical direction is expected to be the major limiter of CTE performance—a

characteristic frequently encountered when working with modern scientific grade CCD detectors. Therefore, to determine the effectiveness of the pre-flushing option on the *Kepler* CCD, as well as several other potential operating modes, only a 20 x 1024 section of the full *Kepler* CCD was simulated, which in turn significantly reduced the run times.

To simulate the *Kepler* image, a star pattern image was created which centered 2 stars randomly over each column, except in column 10 where the stars were specifically centered at rows 250 and 990. Each star was assumed to have a two-dimensional Gaussian shape and was assumed to cover a 5 x 5 pixel aperture. Once the image was setup 5 different runs were made representing different CCD configurations at each of 4 different signal levels for the two stars in column 10. The 4 signal levels (300k, 50k, 10k, and 1ke^-) were chosen to bound the mini-channel capacity (20ke^-), thereby allowing the effectiveness of the mini-channel option to be evaluated.

The first configuration has all options (i.e., proportional loss, trap simulation, dark signal, background signal, image transfer smear, mini-channel, and pre-flushing) turned off and the resultant image is used as a reference for the other 5 configurations. The second configuration enables only the proportional loss CTE model, which applies a fixed CTE value per pixel of 0.999920 to every pixel. The CTE value was determined using the model by Gallagher [5] and the parameters in Table 1. The images produced in configuration two would result with the assumption that every pixel had the same level of CTE performance. The third option enables all options except the proportional loss CTE model, mini-channel, and pre-flushing. The fourth, fifth, and sixth configurations are all based on the third configuration but selectively enable the mini-channel (configuration 4), vertical pre-flushing (configuration 5), and both the mini-channel and pre-flushing (configuration 6).

The results from all modeling runs are shown in Figure 5. Only the image content of rows 986 through 1004 (for column 10) is shown in the Figure 5, because it is only the distortion of the star centered at row 990 (in column 10) that is being evaluated here. Since the *Kepler* application is tasked with performing accurate relative photometry, the two metrics used to evaluate the output of each simulation run were (1) the signal displaced out of the initial 5 pixel aperture (rows 988 through 992), and (2) the signal displaced out of the 988 to 998 aperture.

The *Kepler* application is unique in that the CTE performance of the CCD is not very demanding when compared to other space-based imaging instruments such as STIS and WFPC2. This is a result of several factors: (1) the system software continually optimizes the dimensions of the aperture used to calculate the signal received from each star, (2) the average background signal in each pixel is relatively high (~200e^-), (3) the integrated signal level for a typical star is significantly larger than levels achieved in low light applications, (4) the application is to stare at the same field of view for 4 years straight so the CCDs are always operating in the steady state condition, and (5) the slow degradation in CTE over time has minimal impact on the relative photometry calculations (i.e., the changes can be normalized out). Even with this relatively high insensitivity to CTE degradation, a high CTE is still desired to minimize the likelihood that two stars on a particular column will smear into one another. Therefore, *Kepler* is planning to operate the CCDs at –90°C using the pre-flushing option.

V. DISCUSSION OF MODELING RESULTS

The modeling results for all configurations are summarized in Figures 5 and 6. By comparing the data in the third and fifth columns at each signal level it can be concluded that the use of pre-flushing can significantly improve CTE performance in proton irradiated CCD detectors. These results confirm the common belief that the passing of a large signal through a cooled CCD ahead of the image

signal can significantly reduce the distortion in the output image. By comparing the data in the third and fourth columns at each signal level it is noted that the use of the mini-channel results in higher image distortion (i.e. higher displaced signal). Upon first consideration this observation may seem to contradict the common belief that mini-channels improve CTE (lower image distortion) at low signal levels, but, as will be shown, this is not the case.

To further investigate the performance of the mini-channel six additional configurations were run at the 1ke- signal level (see Figure 6). The effectiveness of the mini-channel can be seen by comparing the results of simulation runs U1A and U4A. In both these runs the results shown are for the first frame off the detector, whereas all other results in Figures 5 and 6 correspond to the fourth frame off the detector. In the U1A run the mini-channel is disabled and the entire star signal is lost. In the U4A run the mini-channel is enabled and only 31% of the signal is lost—demonstrating a significant improvement. The reason the mini-channel for all other configurations (runs) appears less effective is due to the fact that the trap population level is allowed to reach steady state. Once steady state is achieved subsequent images (from the same constant scene) will have significantly improved CTE performance. The proposed *Kepler* program is somewhat unique in its application, that is it stares at the same image for 4 years, and the reader is cautioned against applying the modeling results present herein for the *Kepler* program to other arbitrary applications. It is more common among imaging applications for dynamic scenes or single exposures to be imaged and in both these cases the first or second frame off the detector should be used. Of additional benefit to *Kepler* is the relatively high background signal level of $200e^-$. This can be seen be comparing runs U2 to U3 or U5 to U6.

For signal levels below the mini-channel capacity ($20ke^-$), the addition (runs R and X) or deletion (runs Q and W) of the mini-channel does not significantly affect the CTE performance. As mentioned previously, this is a result of the fact that the traps have reached a steady state condition. At signal levels higher than the mini-channel capacity, the addition of the mini-channel (runs D and K) results in lower CTE performance (when compared to no mini-channel runs C and J). This phenomenon is believed to occur for two reasons. First, for signal levels at or below the mini-channel capacity, the CCD with no mini-channel will keep more traps filled (in steady state) compared to the CCD with a mini-channel. Subsequently, when a large signal (i.e., one greater than the mini-channel capacity) passes through the mini-channel CCD it will interact with more traps compared to the same signal passing through a CCD with no mini-channel. The second reason, as indicated in Figure 1, comes from the assumption that the addition of the mini-channel results in a net increase of storage volume within the buried channel over the no mini-channel case.

During the model validation period it became clear that the particular method used to arrive at a measured CTE value can significantly affect the reported result. Dynamic versus staring applications and low signal versus high signal applications require different measurement methods. For example, when using cosmic ray hits to estimate CTE, the calculated value may be too pessimistic (i.e., lower than will be encountered in the application) because a smaller percentage of traps will be populated relative to the application. For the *Kepler* detector, a steady state output image was not achieved until at least two to three complete frames were read out. One obvious conclusion from these points is that the method chosen to measure or model CTE should match, as closely as possible, the normal operating mode of the detector. For example, using an Fe^{55} source to quantify the CTE on a CCD detector that will be acquiring very low signal images is probably a good choice. Conversely, using the same source to quantify the CTE on a detector that will be acquiring high signal images may yield misleading results.

One additional conclusion reached from the data in Figure 5 is that the use of a constant CTE for all pixels (i.e. the

Proportional Loss CTE Model option) can result in misleading results. Generally speaking, it is believed the imaging results from the use of such models will likely be too pessimistic in predicting image distortion or MTF.

Finally, readers are cautioned against extrapolating the modeling results presented for the static-scene *Kepler* CCD to any other dynamic or static-scene applications, due to the strong dependencies on signal level, scene content, clocking, temperature, and potential differences in CCD architecture and radiation environments. The model described in this paper can be tailored for these parameters and can properly deal with the differences encountered between static and dynamic scenes. Differences in any of these parameters can significantly alter the resultant output images and accordingly it is recommended that a full simulation be performed for each CCD application.

VI. FUTURE ENHANCEMENTS TO MODEL

While the modeling results performed to date appear to be in good agreement with measured results, further comparisons need to be performed to validate specific portions of the model. For example, the present function used to describe the signal level dependency on trap exposure was arrived at empirically by comparing the measured and modeled CTE data from only one ground-based radiation experiment. Accordingly, additional verification and refinement of the function is warranted. To date, this task has been somewhat hampered by a lack of detailed knowledge regarding the exact capacity of the mini-channels and/or accurate knowledge of the radiation exposures and resultant trap densities. Adding a dwell time dependency on trap exposure density and including a signal level dependency on the capture time constant [13] should also be considered. Finally, fringing field effects [11] are not presently accounted for in this model and could be added to better simulate the transport of charge and the distribution of emitted signal from barrier electrodes. However, the potential gain in accuracy by adding such features needs to be weighed against the resultant increase in simulation time.

VII. CONCLUSION

A software model has been developed that accurately accounts for charge transfer efficiency in proton irradiated CCD-based detectors. All significant phenomena are simulated, except as discussed in VI, and a comparison to existing data and models provides some confidence that this modeling approach can produce more accurately and more realistically predictions of real world performance in CCD-based detectors than previous models.

VIII. REFERENCES

[1] J. Janesick, G. Soli, T. Elliott, and S. Collins, "The effects of proton damage on charge-coupled devices," in Charge-Coupled Devices and Solid State Optical Detectors II, Proc. SPIE, Vol. 1447, pp. 87-108, 1991.

[2] C. D. Dale, B. Cummings, L. Shamey, and A. Holland, "Displacement Damage Effects in Mixed Particle Environments for Shielded Spacecraft CCDs," IEEE Trans. Nucl. Sci., Vol. 40, No. 6, pp. 1628-1637, Dec. 1993.

[3] I. H. Hopkins, G. R. Hopkinson, and B. Johlander, "Proton-induced Charge Transfer Degradation in CCDs for Near-Room Temperature Applications," IEEE Trans. Nucl. Sci., Vol 41, No. 6, pp. 1984-1991, Dec. 1994.

[4] G. R. Hopkinson, C. J. Dale, and P. W. Marshall, "Proton Effects in Charge-Couppled Devices," IEEE Trans. Nucl. Sci., Vol. 43, No. 2, pp. 614-627, April 1996.

[5] D. Gallagher, R. Demara, G. Emerson, W. Frame, and A. Delamere, "Monte-Carlo Model for Describing Charge Transfer In Irradiated CCDs, Proceedings of SPIE, Solid State Sensor Arrays: Development and Applications II, Vol. 3301, 1998.

[6] J. Janesick, "Scientific Charge-Coupled Devices," Published by SPIE, ISBN 0-8194-3698-4, pp. 453, 2001.

[7] W. J. Borucki, E. W. Dunham., D. G. Koch, W. D. Cochran, J. A. Rose, K. Cullers, A. Granados, and J. M. Jenkins, FRESIP: A Mission to Determine the Character and Frequency of Extra-Solar Planets Around Solar-Like Stars, Astrophysics & Space Science, 241, 111-134,(1996).

[8] A. M. Mohsen, and M. F. Tompsett, "The Effects of Bulk Traps on the Performance of Bulk Channel Charge-Coupled Devices," IEEE Trans. Elect. Dev., Vol. ED-21, No. 11, pp. 701-712, Nov. 1974.

[9] Space Telescope Science Institute, "STIS Instrument handbook for Cycle 10," dated 5/10/01. (available through the internet)

[10] M. Robbins, “The Radiation Damage Performance of Marconi CCDs,"”Marconi Applied Technologies, Technical Note: S&C906/424, Dated Feb. 17, 2000. (available upon request)

[11] E. K. Banghart, J. P. Lavine, E. A. Trabka, E. T. Nelson, and B. C. Burkey, “A Model for Charge Transfer in Buried-Channel Charge-Coupled Devices at Low Temperature,” IEEE Trans. Elect. Dev., Vol. 38, No. 5, pp. 1162-1174, May 1991.

[12] C. J. Dale, L. Chen, P. J. Marshall, and E. A. Burke, “A Comparison of Monte Carlo and Analytic Treatments of Displacement Damage in Si Microvolumtes,” IEEE Trans. Nucl. Sci., Vol. 41, No. 6, pp. 1974-1983, Dec. 1994.

[13] M. Robbins, T. Roy, and S. Watts, “Degradation of the charge transfer efficiency of a buried channel charge coupled device due to radiation damage by a beta source,” Brunel University, Physics Department Document BRU/DDG/109, Sept. 1991.

Figure 1 Relative trap exposure functions for both the mini-channel and non mini-channel scenarios as a function of relative signal level. The discontinuity in the mini-channel curve has been included to account for the assumed increase in volume attributed to the mini-channel.

Figure 2 Examples of several electron trap and emission scenarios: (a) a signal electron, from either incident photons or dark signal, is captured under a barrier phase, (b) signal electrons are trapped and emitted under storage phases, and (c) a signal electron is emitted under a barrier phase and is divided between the two adjacent storage phases (i.e. phases 2 and 3 shown and phases 2 and 3 (not shown) to the right of the right most phase 1 electrode).

Figure 3 Execution flow diagram of the Trapper modeling program. The program was written in standard C and can be run on any computer platform supporting a standard C compiler. Items with rounded corners represent features that can be edited and/or selectively enabled or disabled. The flow diagram has been simplified to more clearly show the execution of the CTE portion of the program. For example, when calculating MTF, an additional loop is added outside of the frame index loop to step through the range of spatial frequencies for the sinusoidal input image.

Figure 4 Block diagram of the CCD to be used on the proposed Kepler Discovery Mission. The architecture is full frame with 27 μm x 27 μm pixels and contains vertical injection and 4-phase CCDs in both the horizontal and vertical directions. 20 light shielded rows (not shown) adjacent to the serial CCD provides a reference for dark signal and image smear removal.

Figure 5 Modeling simulation results for the Kepler CCD. Six different CCD configurations were used at each of four different signal levels (i.e. 300k, 50k, 10k, and 1k e-). The first configuration at each signal level disables all options other than imaging to arrive at an ideal output image. The second option enables the standard proportional loss CTE model, which assumes a mini-channel is present. The third configuration enables trap capture and emission and all secondary imaging sources (e.g. dark signal generation, background scene (stars), and image transfer smear). The fourth, fifth, and sixth configurations are all based on the third configuration but selectively enable the mini-channel (configuration 4), vertical pre-flushing (configuration 5), and both the mini-channel and pre-flushing (configuration 6). The pixel data shown is for rows 986 through 1004 at column 10 and has the background signal (offset level) subtracted off to enhance the readability of the resultant image signal. The percentage of star signal lost is calculated by comparing the signal summed in each aperture to the summed signal for the ideal case (configuration 1 for each of the four signal levels). The image signal in all cases was taken from the fourth image read off the CCD during the simulation to ensure a steady state condition was reached. Two stars of varying intensity were centered in each column at random row locations. For column 10, one star was centered at row 990 (with intensity as shown) and the other was centered over row 250 with approximately half the intensity.

Figure 6 Additional modeling simulation results for the Kepler CCD. Six different CCD configurations were used at a signal level of 1k e- to investigate the effectiveness of the mini-channel. Note that run U1A is the first frame out of run U1 and run U4A is the first fame out of run U4. All other data shown corresponds to the fourth frame out of each run. The first three configurations (U1, U2, and U3) have the mini-channel disabled (off) and the last three runs have the mini-channel enabled. Comparing run U1A to U4A it is seen that the mini-channel yields a significant improvement in CTE performance when the trap population level is not in steady state. However, once steady state is achieved the existence or absence of the mini-channel does not significantly alter the CTE performance, as indicated in runs U3 and U4.

Table 1 Input parameters used to simulate the Kepler CCD. The CTE value listed, which was produced using the analytical equation presented by Gallagher et al. [5] and the radiation parameters (e.g. trap densities) shown, was used to generate the "Proportional Loss CTE Model" results shown in Figure 5.

Figure 1

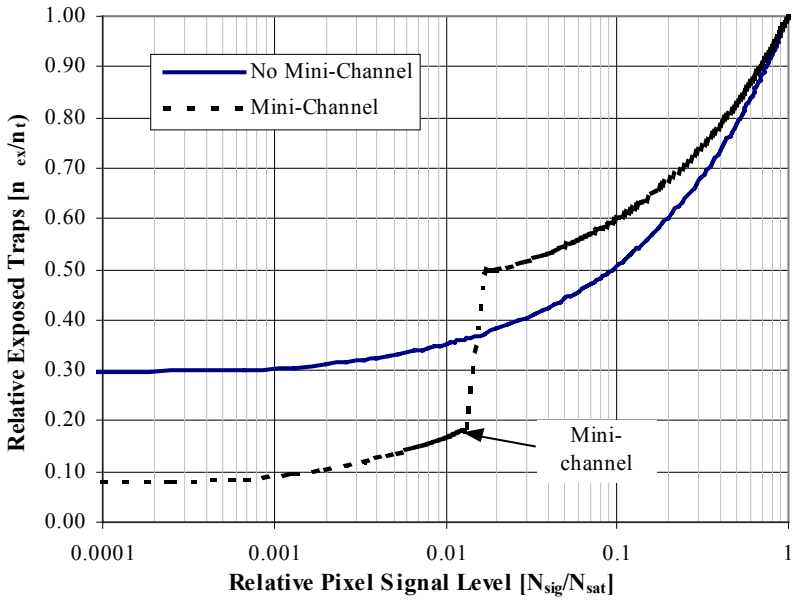
1.00
0.90
0.80
0.70
0.60
0.50
0.40
0.30
0.20
0.10
0.00
No Mini-Channel
Mini-Channel
Mini-
channel
Relative Exposed Traps [n ex/nt]
0.0001
0.001
0.01
0.1
1
Relative Pixel Signal Level [Nsig/Nsat]

Figure 2

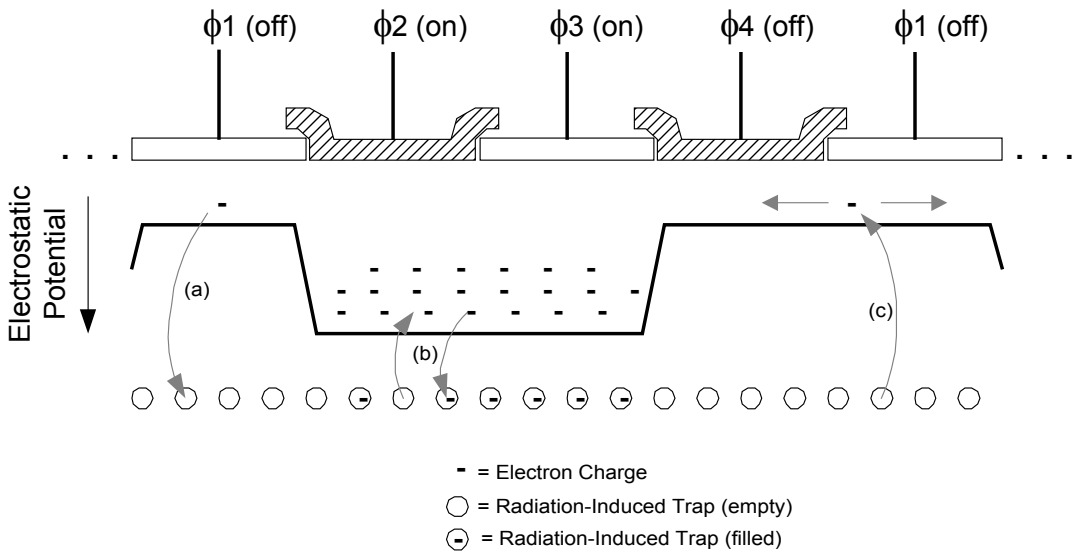
ϕ1 (off)
ϕ2 (on)
ϕ3 (on)
ϕ4 (off)
ϕ1 (off)
Electrostatic Potential
(a)
(b)
(c)
- = Electron Charge
◯ = Radiation-Induced Trap (empty)
⊖ = Radiation-Induced Trap (filled)

Figure 3

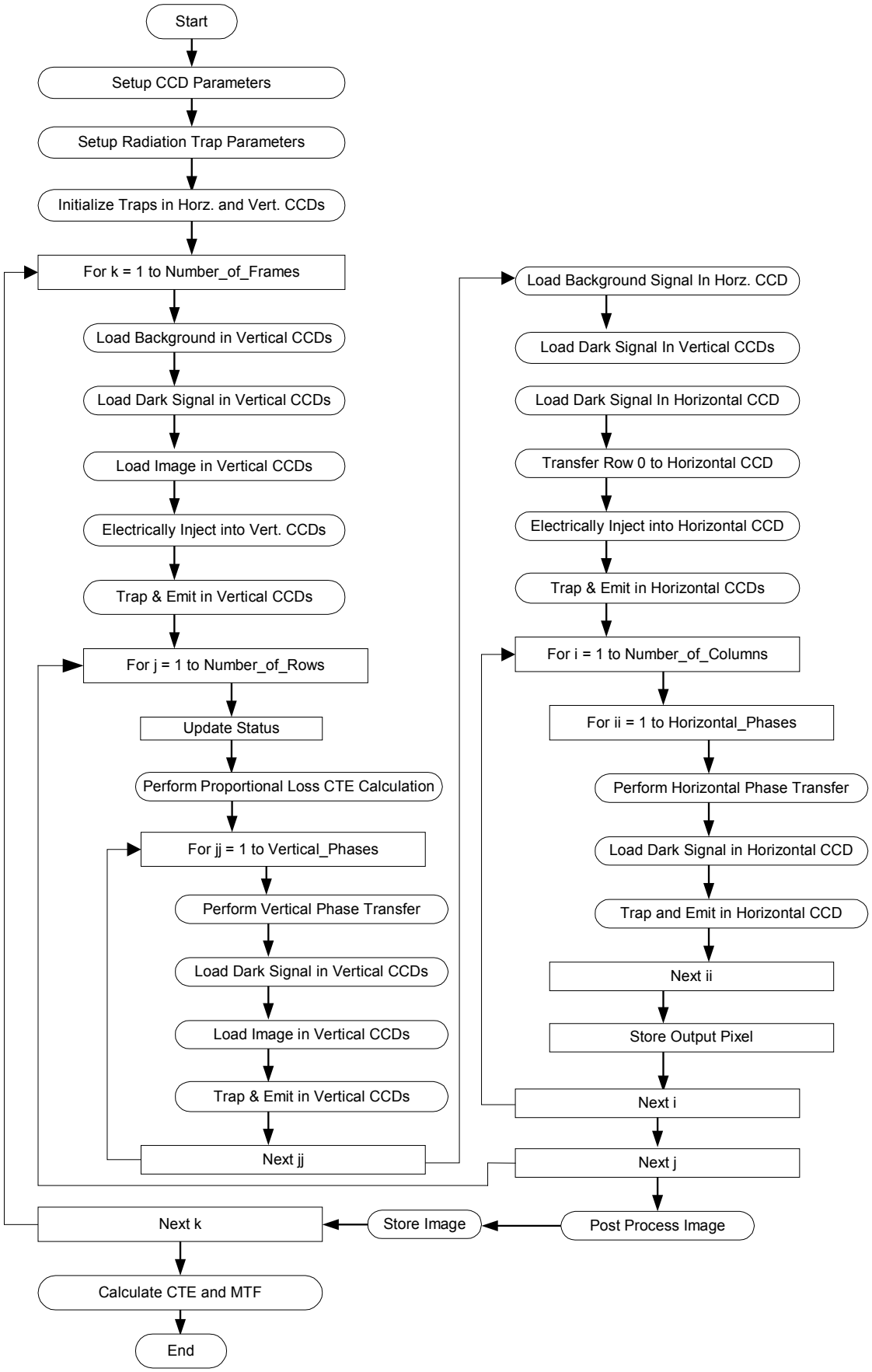
Start
Setup CCD Parameters
Setup Radiation Trap Parameters
Initialize Traps in Horz. and Vert. CCDs
For k = 1 to Number_of_Frames
Load Background in Vertical CCDs
Load Dark Signal in Vertical CCDs
Load Image in Vertical CCDs
Electrically Inject into Vert. CCDs
Trap & Emit in Vertical CCDs
For j = 1 to Number_of_Rows
Update Status
Perform Proportional Loss CTE Calculation
For jj = 1 to Vertical_Phases
Perform Vertical Phase Transfer
Load Dark Signal in Vertical CCDs
Load Image in Vertical CCDs
Trap & Emit in Vertical CCDs
Next jj
Load Background Signal In Horz. CCD
Load Dark Signal In Vertical CCDs
Load Dark Signal In Horizontal CCD
Transfer Row 0 to Horizontal CCD
Electrically Inject into Horizontal CCD
Trap & Emit in Horizontal CCDs
For i = 1 to Number_of_Columns
For ii = 1 to Horizontal_Phases
Perform Horizontal Phase Transfer
Load Dark Signal in Horizontal CCD
Trap and Emit in Horizontal CCD
Next ii
Store Output Pixel
Next i
Next j
Post Process Image
Store Image
Next k
Calculate CTE and MTF
End

Figure 5

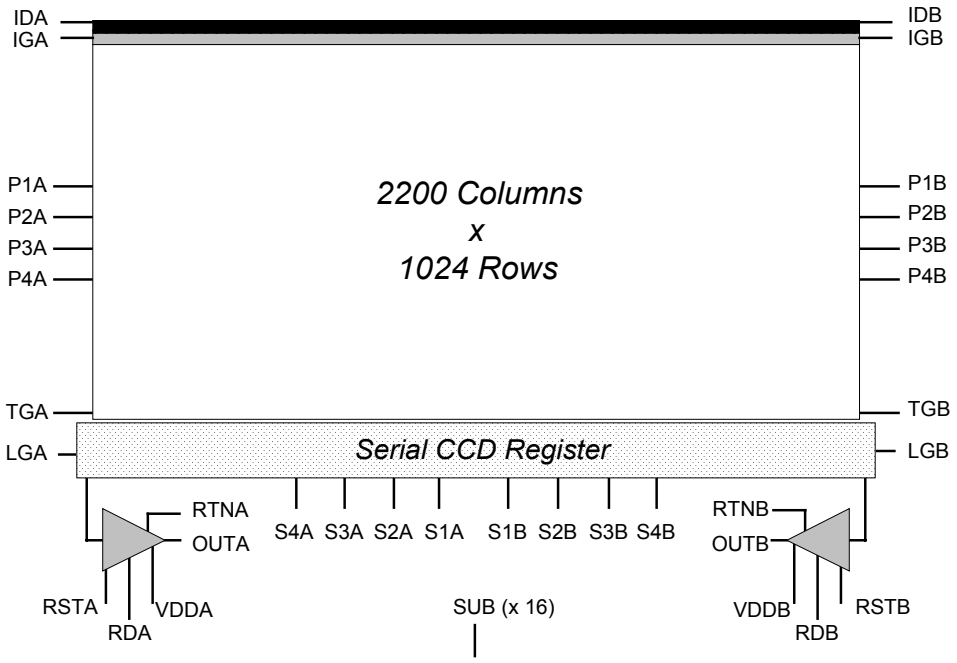
IDA
IGA
IDB
IGB
2200 Columns
x
1024 Rows
P1A
P2A
P3A
P4A
P1B
P2B
P3B
P4B
TGA
TGB
LGA
Serial CCD Register
LGB
RTNA
OUTA
S4A S3A S2A S1A S1B S2B S3B S4B
RTNB
OUTB
RSTA
RDA
VDDA
SUB (x 16)
VDDB
RDB
RSTB

Figure 6

Simulation Run →	Simulation Results - Portion of Readout Image with Background Signal Removed [e⁻]																							
Simulation Option	*A*	*B*	*C*	*D*	*E*	*F*	*G*	*H*	*J*	*K*	*L*	*M*	*N*	*P*	*Q*	*R*	*S*	*T*	*U*	*V*	*W*	*X*	*Y*	*Z*
Integrated Signal Level [e-]	**300,000**	**300,000**	**300,000**	**300,000**	**300,000**	**300,000**	**50,000**	**50,000**	**50,000**	**50,000**	**50,000**	**50,000**	**10,000**	**10,000**	**10,000**	**10,000**	**10,000**	**10,000**	**1,000**	**1,000**	**1,000**	**1,000**	**1,000**	**1,000**
Proportional Loss CTE Model	**OFF**	**ON**	**OFF**	**OFF**	**OFF**	**OFF**	**OFF**	**ON**	**OFF**	**OFF**	**OFF**	**OFF**	**OFF**	**ON**	**OFF**	**OFF**	**OFF**	**OFF**	**OFF**	**ON**	**OFF**	**OFF**	**OFF**	**OFF**
Trap Capture and Emission	**OFF**	**OFF**	**ON**	**ON**	**ON**	**ON**	**OFF**	**OFF**	**ON**	**ON**	**ON**	**ON**	**OFF**	**OFF**	**ON**	**ON**	**ON**	**ON**	**OFF**	**OFF**	**ON**	**ON**	**ON**	**ON**
Dark Signal Generation	**OFF**	**OFF**	**ON**	**ON**	**ON**	**ON**	**OFF**	**OFF**	**ON**	**ON**	**ON**	**ON**	**OFF**	**OFF**	**ON**	**ON**	**ON**	**ON**	**OFF**	**OFF**	**ON**	**ON**	**ON**	**ON**
Background Signal	**OFF**	**OFF**	**ON**	**ON**	**ON**	**ON**	**OFF**	**OFF**	**ON**	**ON**	**ON**	**ON**	**OFF**	**OFF**	**ON**	**ON**	**ON**	**ON**	**OFF**	**OFF**	**ON**	**ON**	**ON**	**ON**
Image Smear	**OFF**	**OFF**	**ON**	**ON**	**ON**	**ON**	**OFF**	**OFF**	**ON**	**ON**	**ON**	**ON**	**OFF**	**OFF**	**ON**	**ON**	**ON**	**ON**	**OFF**	**OFF**	**ON**	**ON**	**ON**	**ON**
Mini-Channel	**OFF**	**ON**	**OFF**	**ON**	**OFF**	**ON**	**OFF**	**ON**	**OFF**	**ON**	**OFF**	**ON**	**OFF**	**ON**	**OFF**	**ON**	**OFF**	**ON**	**OFF**	**ON**	**OFF**	**ON**	**OFF**	**ON**
Vertical Injection (pre-flush)	**OFF**	**OFF**	**OFF**	**OFF**	**ON**	**ON**	**OFF**	**OFF**	**OFF**	**OFF**	**ON**	**ON**	**OFF**	**OFF**	**OFF**	**OFF**	**ON**	**ON**	**OFF**	**OFF**	**OFF**	**OFF**	**ON**	**ON**
Row Number (direction of transfer) 1004	0	0	0	0	0	0	0	0	0	0	0	0	0	0	0	0	0	0	0	0	0	0	0	0
1003	0	0	0	0	0	0	0	0	0	0	0	0	0	0	0	0	0	0	0	0	0	0	0	0
1002	0	0	0	0	0	0	0	0	0	0	0	0	0	0	0	0	0	0	0	0	0	0	0	0
1001	0	0	0	0	0	0	0	0	0	0	0	0	0	0	0	0	0	0	0	0	0	0	0	0
1000	0	0	0	0	0	0	0	0	0	0	0	0	0	0	1	0	0	0	0	0	0	0	0	0
999	0	0	0	0	0	0	0	0	0	0	0	0	0	0	1	0	0	0	0	0	0	0	0	0
998	0	0	0	0	0	1	0	0	0	0	0	0	0	0	1	0	0	0	0	0	0	0	0	0
997	0	0	0	2	0	3	0	0	0	0	0	0	0	0	1	0	0	0	0	0	0	0	0	0
996	0	0	0	51	0	52	0	0	0	2	0	2	0	0	1	0	0	0	0	0	0	0	0	0
995	0	1	0	92	0	92	0	0	0	50	0	50	0	0	1	0	0	0	0	0	0	0	0	0
994	0	25	0	164	0	164	0	4	0	89	1	89	0	1	1	1	1	1	0	0	0	0	0	0
993	0	747	106	317	106	318	0	124	26	167	26	166	0	25	10	17	10	17	0	2	2	2	2	2
992	5,495	14,037	5,849	6,299	5,849	6,300	916	2,339	1,064	1,235	1,065	1,234	183	468	242	259	242	259	18	47	32	35	32	35
991	110,364	124,222	110,684	110,623	110,684	110,622	18,394	20,704	18,523	19,071	18,524	19,070	3,679	4,141	3,735	3,754	3,735	3,754	368	414	381	388	382	388
990	300,000	285,239	298,082	298,433	298,082	298,434	50,000	47,540	49,221	45,317	49,609	47,195	10,000	9,508	9,661	9,551	9,943	9,924	1,000	951	913	876	986	980
989	110,364	102,369	109,419	107,539	109,419	107,907	18,394	17,062	17,956	18,196	18,245	18,193	3,679	3,412	3,446	3,482	3,620	3,597	368	341	291	311	354	352
988	5,495	5,077	5,383	5,387	5,383	5,384	916	846	876	883	890	880	183	169	169	169	175	174	18	17	13	17	17	18
987	0	0	2	3	2	0	0	0	0	2	0	0	0	0	1	1	0	0	0	0	0	0	0	0
986	0	0	2	3	2	0	0	0	0	2	0	0	0	0	1	1	0	0	0	0	0	0	0	0
Offset Level	0	0	471	471	471	475	0	0	246	246	249	251	0	0	209	209	213	214	0	0	201	201	205	206
Signal in 5 Pixel Window	531,717	530,945	529,416	528,281	529,416	528,647	88,620	88,491	87,641	84,701	88,332	86,572	17,724	17,698	17,253	17,215	17,715	17,709	1,772	1,770	1,630	1,627	1,772	1,772
Signal in 11 Pixel Window	531,717	531,717	529,523	528,907	529,523	529,276	88,620	88,619	87,667	85,010	88,361	86,878	17,724	17,724	17,266	17,234	17,726	17,728	1,772	1,772	1,634	1,629	1,774	1,776
% of Sig. Lost From 5 Pixel Window		**0.15**	**0.43**	**0.65**	**0.43**	**0.58**	%	**0.15**	**1.10**	**4.42**	**0.32**	**2.31**	%	**0.15**	**2.66**	**2.87**	**0.05**	**0.09**	%	**0.15**	**8.01**	**8.22**	**0.04**	**0.00**	%
% of Sig. Lost From 11 Pixel Window (988 to 998)		**0.00**	**0.41**	**0.53**	**0.41**	**0.46**	%	**0.00**	**1.07**	**4.07**	**0.29**	**1.96**	%	**0.00**	**2.59**	**2.76**	**-0.01**	**-0.02**	%	**0.00**	**7.81**	**8.08**	**-0.10**	**-0.18**	%

Figure 7

Simulation Run									
Simulation Option		*U1*	*U1A**	*U2*	*U3*	*U4*	*U4A**	*U5*	*U6*
Integrated Signal Level [e-]		**1,000**	**1,000**	**1,000**	**1,000**	**1,000**	**1,000**	**1,000**	**1,000**
Proportional Loss CTE Model		**OFF**	**OFF**	**OFF**	**OFF**	**OFF**	**OFF**	**OFF**	**OFF**
Trap Capture and Emission		**ON**	**ON**	**ON**	**ON**	**ON**	**ON**	**ON**	**ON**
Dark Signal Generation		**OFF**	**OFF**	**ON**	**ON**	**OFF**	**OFF**	**ON**	**ON**
Background Signal		**OFF**	**OFF**	**OFF**	**ON**	**OFF**	**OFF**	**OFF**	**ON**
Image Smear		**ON**	**ON**	**ON**	**ON**	**ON**	**ON**	**ON**	**ON**
Mini-Channel		**OFF**	**OFF**	**OFF**	**OFF**	**ON**	**ON**	**ON**	**ON**
Vertical Injection (pre-flush)		**OFF**	**OFF**	**OFF**	**OFF**	**OFF**	**OFF**	**OFF**	**OFF**
Row Number (direction of transfer)	1004	0	0	0	0	0	0	0	0
	1003	0	0	0	0	0	0	0	0
	1002	0	0	0	0	0	0	0	0
	1001	0	0	0	0	0	0	0	0
	1000	0	0	0	0	0	0	0	0
	999	0	0	0	0	0	0	0	0
	998	0	0	0	0	0	0	0	0
	997	0	0	0	0	0	0	0	0
	996	0	0	1	0	0	0	1	0
	995	1	0	1	0	1	1	1	0
	994	2	0	2	0	3	2	3	0
	993	8	0	8	2	9	9	9	2
	992	44	0	44	32	44	43	44	35
	991	383	0	384	381	390	389	390	388
	990	886	0	886	913	856	786	857	876
	989	230	0	231	291	281	0	282	311
	988	5	0	5	13	8	0	9	17
	987	0	0	0	0	0	0	0	0
	986	0	0	0	0	0	0	0	0
Offset Level		1	0.28	1	201	1	1	1	201
Signal in 5 Pixel Window		1,548	0	1,550	1,630	1,580	1,218	1,582	1,627
Signal in 11 Pixel Window		1,559	0	1,562	1,634	1,593	1,231	1,596	1,629
% Lost From 5 Pixel Window		**12.68**	**100.00**	**12.55**	**8.01**	**10.88**	**31.28**	**10.74**	**8.22** %
% Lost From 11 Pixel Window		**12.06**	**100.00**	**11.86**	**7.81**	**10.15**	**30.57**	**9.94**	**8.08** %
(988 to 998)		* Data taken from 1st frame, all other data taken from 4th frame							

Table 1

Parameter		Value	Units
Number of Active Columns		2200	#
Number of Active Rows		1004	#
Number of Light Shielded Rows		20	#
Pixel Pitch (horizontal and vertical)		27	µm
Mini-Channel Width		5	µm
Depth of Storage Region		0.20	µm
Width of Horizontal CCD		40.0	µm
Mini-Channel Capacity		20	ke^-
Vertical CCD Pixel Capacity		1,000	ke^-
Horizontal CCD Charge Capacity		1,200	ke^-
Signal Injected into Vertical CCD		750	ke^-
Vertical/Horizontal CCD Architecture		4	Phase
Total NIEL after 4 years in space (2x)		4.4E+7	MeV/g
Operating Temperature		-90	°C
O-V Trap:	Density	1.0E+10	# / cm^3
	E_{gap}	0.168	eV
	$\sigma_n \cdot X_n$	5E-16	cm^2
	τ_e	1.82E-7	s
	τ_c	911	ns
V-V Trap:	Density	1.76E+10	# / cm^3
	E_{gap}	0.300	eV
	$\sigma_n \cdot X_n$	5E-16	cm^2
	τ_e	7.86E-4	s
	τ_c	911	ns
P-V Trap:	Density	1.01E+11	# / cm^3
	E_{gap}	0.440	eV
	$\sigma_n \cdot X_n$	7E-16	cm^2
	τ_e	4.02	s
	τ_c	650	ns
Dark Signal Generation Rate (-90°C)		2.2E-6	nA / cm^2
CTE (at 1620 e^- signal level)		0.999920	per pixel
Integration Period		2.5	s
Horizontal CCD Clocking Period		333.3	ns
Vertical CCD Clock Period		483.6	µs
Vert.-to-Horz. CCD Transfer Period		133	µs
Background Signal Level		200	e^-
Star Images Centered Over Column 10 (at rows 250 & 990)		2	#
Intensity of Column 10 Stars		Variable	#
Radius of All Star Images		5	Pixels
Shape of All Star Images		Gaussian	
Star Images Centered Over Other Columns		2	#
Intensity of Other Column Stars		Scaled to col. 10 stars	#